Process Mechanism in Shape Adaptive Grinding (SAG), for Application to Aspheric X-Ray Mirror Molding Dies

Yoshiharu Namba, Anthony Beaucamp

Richard Freeman (Zeeko LTD)

Shape Adaptive Grinding (SAG) is a novel process for freeform machining of difficult materials such as ceramics and hard metals. Despite low stiffness equipment from the machining equipment, due to the semi-elasticity of the tools, ductile mode grinding can be achieved with high surface finish. The SAG process mechanism was investigated by studying how the size and shape of the pellet bonded abrasives evolve over time, and by measuring grinding forces for a variety of process parameters. The micro-topography was measured at various level of magnification and found to be consistently between 0.3 and 0.5 nm rms. It is expected that aspheric mandrels with form accuracy below 100nm P-V and micro-roughness below 0.5 nm rms will be produced in the future by this method.

1. Introduction

Shape Adaptive Grinding (SAG) is an innovative and low-cost machining method that we recently proposed[1]. Difficult ceramic materials can be machined by SAG from a very rough condition (above 1 μm Ra) down to a very fine optical surface finish (below 0.5 nm Ra). The basic principle of SAG machining is shown in Fig. 1. It can be described as "semi-elasticity": through the use of an elastic tool, general compliance is maintained between the grinding tool and freeform surface over a sub-aperture contact area of the workpiece, but hard contact at relatively smaller scale is simultaneously achieved thanks to rigid pellets covering the surface of the elastic tool. In these conditions, effective grinding can take place (rather than polishing resulting from a soft contact).

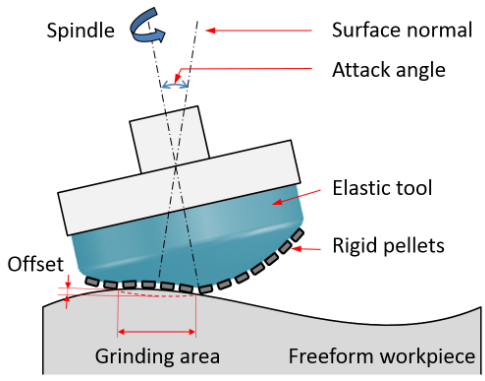

Fig.1 Principle of Shape Adaptive Grinding (SAG)

Some attractive characteristics of this new machining process are listed as follows:

1. Low manufacturing cost of the tooling.
2. Applicability to any aspheric or freeform shape, due to the adaptive nature of the grinding contact area.
3. Deployment on “low-cost” CNC machinery (overall stiffness of the apparatus does not affect this “semi-elastic” process).
4. Ability to achieve ductile-mode grinding with smaller abrasive grit sizes.
5. Ability to maintain high removal rates whilst achieving low surface roughness (when compared to other ultra-precision grinding methods[2)].

For these reasons, a new method for manufacturing CVD SiC coated graphite mandrels for application to X-ray mirrors was investigated. The manufacturing principle is shown in Fig. 2: A high-speed milling machine is used to cut the aspheric mandrel shape into a block of graphite, a material that is inexpensive to acquire and machine (at least one order of magnitude cheaper than fused silica). The cut mandrel is then placed inside a reactor, where a coating of silicon carbide is deposited by CVD process.

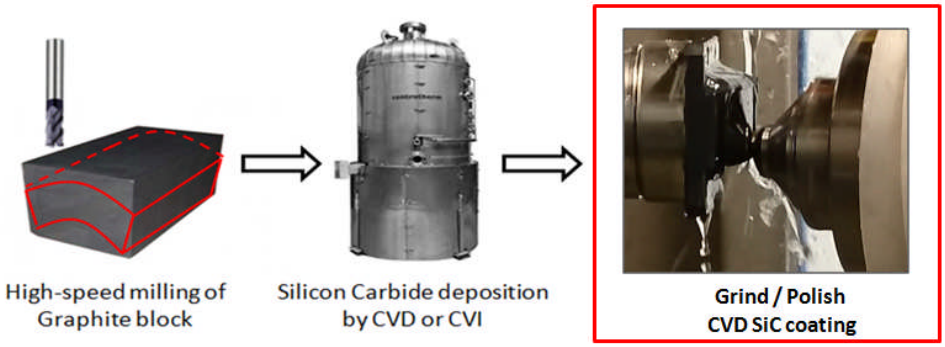

Fig.2 Fabrication chain to produce hard X-ray mandrels from graphite coated with SiC

The grinding characteristics of the SAG process were studied using confocal laser microscopy to observe pellets and abrasives, dynamometry to study the grinding forces as function of the various process parameters, and observations of the ground micro-topography by whitelight interferometry and atomic force microscopy. The aims of this study included understanding: (1) how stably this process behaves over time, (2) how the various process parameters correlate with grinding forces, (3) how the chip thickness correlates to the condition of machined surfaces, and (4) whether a high degree of surface finish can be achieved at various levels of magnification.

2. Study of SAG Tool

2.1 Experimental Method

The first set of experiments consisted of investigating the diamond abrasives bound inside SAG pellets, in order to gather basic information about the number and shape of grinding edges,

and monitor their evolution over time. For this purpose, fresh grinding tools were prepared, and used to grind graphite coated with CVD silicon carbide for a number of successive runs totaling 10 hours. The grinding parameters are summarized in Table 1. In-between grinding runs, the tool was inspected with a confocal laser microscope at various magnifications (5x, 20x, 100x).

Table 1 Process Parameters of SAG Tool

Substrate	Graphite coated with CVD SiC
Tool type	Shape adaptive grinding
Tool radius	10 mm
Tool path mode	Raster
Attack angle	15 deg
Grinding feed	150 mm/min
Spindle rotation	1500 rpm
Total grinding time	10 hrs
Abrasives	Diamond
Grain size	3, 9, 40 μm
Pellet material	Nickel and resin

2.2 Basic Observations and Statistics

Figure 3 shows a photograph and micrographs of a 9 μm nickel bond grinding tool at various magnifications including 5x, 20x and 100x. As can be seen in Fig. 3(b), the tool has a structure consisting of a woven metallic mesh above which circular pellets 0.5 mm in diameter were deposited by electroplating (resin pellets are approximately 50% smaller than nickel pellets). As can be seen in Fig. 3(c), the surface of each pellet consists of circular sub-nodules approximately 0.08 mm in diameter (resin pellets are smaller and thus do not have nodules). As can be seen in Fig. 3(d), diamonds are embedded inside each nodule.

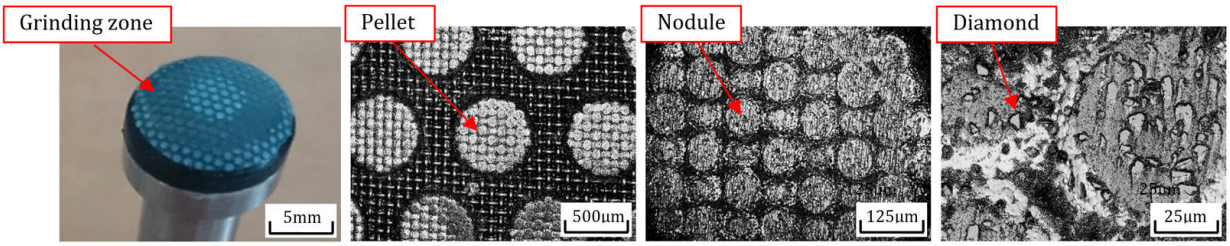

(a) Photograph (b) Micrograph (5x) (c) Micrograph (20x) (d) Micrograph (100x)

Fig.3 Block of fused silica, before and after grinding of the freeform shape

Figure 4 shows 100x magnification micrographs for each of the pellet types used in this experiment (3 μm and 9 μm bonded in resin pellets, as well as 9 μm and 40 μm bonded in nickel pellets) after 30 min of grinding.

By analyzing a large number of micrographs, it was possible to assess the average density of diamond on the pellets. The total number of diamonds in contact with the surface during grinding could then be estimated by integrating across the grinding area, as shown in Table 2.

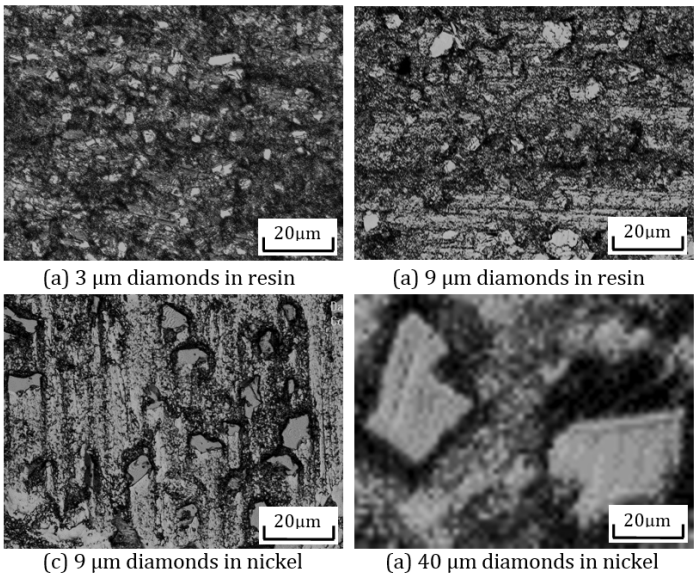

(a) 3 μm diamonds in resin (a) 9 μm diamonds in resin

(c) 9 μm diamonds in nickel (a) 40 μm diamonds in nickel

Fig.4 Micrographs of various pellets after 30 min grinding (100x)

Table 2 Statistics over 5 mm² grinding contact area (tool radius of 10 mm, tool offset of 0.3 mm) for various SAG pellet types.

Tool type	Pellets	Nodules	Diamonds
3 μm resin bonded	25	N/A	21,875 (25 x 875)
9 μm resin bonded	25	N/A	2,750 (25 x 110)
9 μm nickel bonded	7	308 (7 x 44)	3,080 (308 x 10)
40 μm nickel bonded	7	308 (7 x 44)	616 (308 x 2)

Individual pellets were profiled in order to determine the grinding condition of the diamonds relative to the workpiece surface. Figure 5 (left) shows a close-up picture of a single diamond, for which the grinding direction goes toward the top-right of the figure. From the sharply flattened appearance of the diamonds, it is evident that most diamonds are contacting the workpiece surface during the grinding operation. At the leading edge of each diamond, there exists a void that corresponds to the pocket through which chips are generated and debris flow around the diamond. At the trailing edge of the diamond, there exists an up-stand of pellet binder material that allows for the existence of a relief angle, as shown in the diagram in Figure 5 (right).

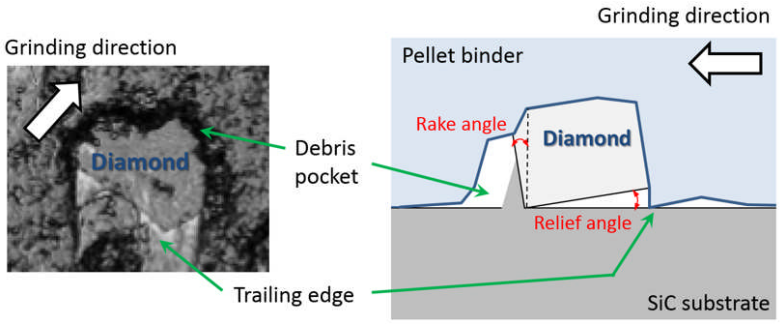

Fig.5 Close-up image of a single diamond (left) and diagram of the corresponding grinding condition (right)

Experimental values of the rake and relief angle were recorded using several micrographs of the 9 μm nickel bond pellets. The resulting distribution curves are shown in Figure 6. The mean values of these distributions were: -13.98 deg for the rake angle, and -6.89 deg for the relief angle.

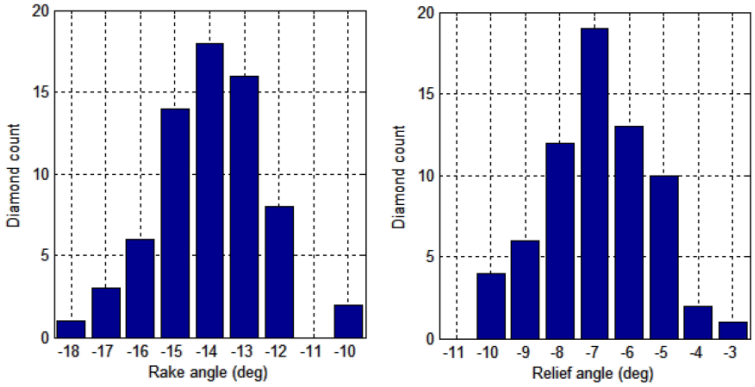

Fig.6 Distribution curves of rake (left) and relief (right) angle

The negative value of the rake angle implies a higher strength of the diamond grinding edges, and can be correlated to the fine ductile, ductile/fracture finishes previously reported in micrographs of ground ceramics[1]. However, such negative angle must also imply high grinding forces and temperature, so the specific grinding energy is expected to be quite large[3]. This aspect is investigated in more details in a following section through measurement of grinding forces.

2.3 Grinding Ratio

Individual pellets were measured before and after the grinding experiments, using a focus depth scanning digital microscope. Figure 7 shows examples of pellet measurements obtained with this equipment.

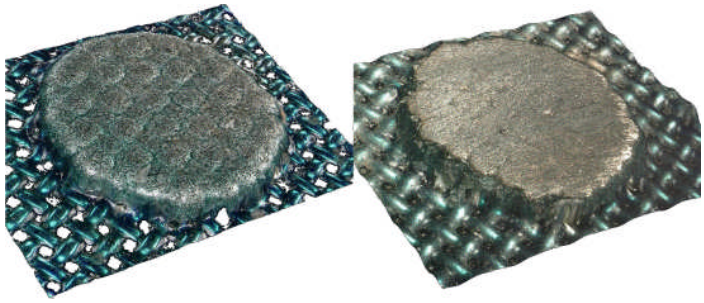

(a) Before grinding (b) After 10 hours

Fig.7 Profile of nickel pellet before and after grinding experiment

By fixing a datum against the underlying metallic mesh, it was possible to measure the absolute pellet height and thus the pellet wear over time. The material removal rate was also measured between grinding experiments using a profilometer. Using this data, it was possible to

determine the grinding ratio defined by the ratio between stock removal of the workpiece and wear of the grinding tool.

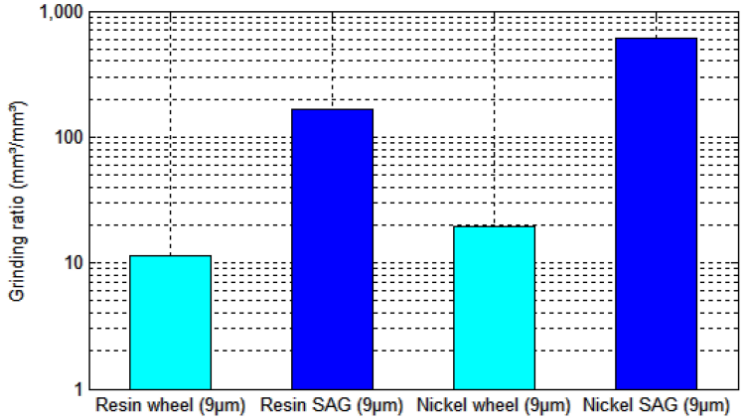

Fig.8 Comparison of grinding ratio between conventional grinding wheels (cyan) and SAG (blue)

Figure 8 shows the grinding ratio for the resin and nickel SAG pellet types in blue. Using a reference from Prof. Inasaki[4], the equivalent ratio for conventional grinding wheels was interpolated and added to the figure in cyan. As can be seen, the grinding ratio of SAG tools is approximately 1 order of magnitude higher than equivalent conventional wheels.

2.4 Equivalent Chip Thickness

In conventional grinding, the equivalent chip thickness can be derived from the macro-scale properties of the grinding equipment. By considering the 2D model of a grinding wheel, Snoeys et al. [5] proposed a macroscopic definition of the equivalent chip thickness h_{eq} [mm] as shown in Eq. 1:

$$h_{eq} = \frac{Z'}{v_s} \qquad (1)$$

where Z' is the stock removal rate [mm²/s], and vs the surface feed of the grinding wheel [mm/s].

In the case of the SAG process, it is possible to derive a more precise model based on microscopic observations and 3D statistical averaging. Microscope observations of the pellets/abrasives were combined with profilometric measurements of the volumetric removal rate, such that the grinding work of individual abrasives could be evaluated, and the equivalent chip thickness could then be derived statistically.

Figure 9 shows the principle of pellet grinding: the grinding area is transversed by a number of pellets Pi moving at various velocities V_i. The pellets are covered with abrasives with average width of grinding edge E_W.

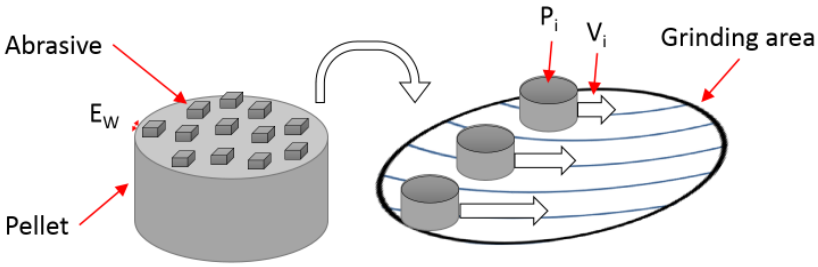

Fig.9 Principle of pellet grinding, used to derive the equivalent chip thickness

The equivalent chip thickness can then be expressed in the form of Eq. 2:

$$h_{eq} = \frac{Q'}{\sum_{i=0}^{n} V_i (E_w A_n)} \qquad (2)$$

where h_{eq} is the equivalent chip thickness [mm], Q' the volumetric removal rate [mm^3/s], Vi the velocity of pellet Pi [mm/s], E_w the average width of grinding edges [mm], and A_n the average number of abrasives per pellet.

Figure 10 shows the resulting statistical computation of equivalent chip thicknesses for various pellet types: below 1 nm for fine 3 μm abrasives, between 1~10 nm for 9 μm abrasives, and above 10 nm for 40 μm abrasives.

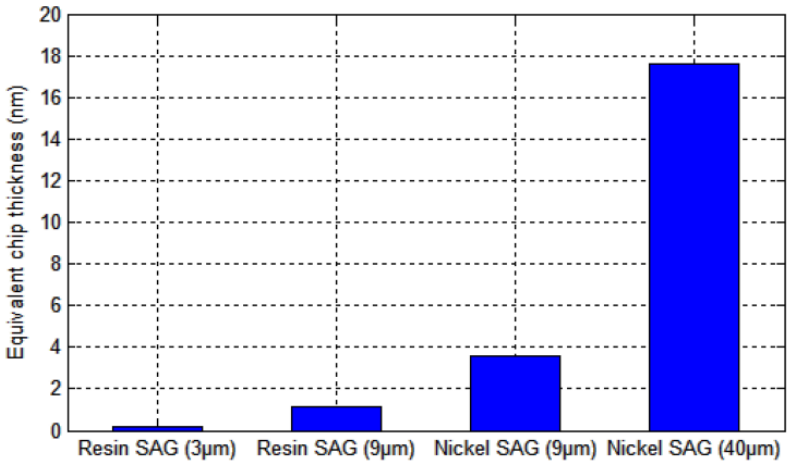

Fig.10 Equivalent chip thickness for the various pellet types

2.5 Grinding Mechanism

In machining of brittle ceramics, the material response is a critical factor influencing the quality of the finished surface. Pioneering studies were conducted by Prof. Yoshikawa[6] on the brittle-ductile behavior of crystal surfaces in finishing operations. In this theoretical model of elasto-plasticity, the size of the stress field is translated into a "machining unit" that is used to classify process mechanisms into four domains. Although this model does not take into account

various factors such as grain boundaries, it has long been regarded as a reference in this field.

An approximation of the machining unit can be obtained by using a damage prediction model. Dobrescu et al[7] have proposed a model of sub-surface damage in grinding ceramics, in which the damage depth and equivalent chip thickness can be related through Eq. 3:

$$\xi^m \sim \alpha K_0 h_g^{1-\varepsilon} \qquad (3)$$

where ξ is the damage depth [mm], the exponent m is in the range 0.5~1.5 for different loading conditions, α is the ratio of the normal to tangential grinding forces, K_0 and ε are constants determined by the material properties, and h_g is the maximum grit depth of cut [mm].

Table 3 shows a classification by SAG pellet type, of the theoretical grinding mechanism derived from Yoshikawa's machining domains, and the actual grinding mode observed in micrographs of ground surfaces (as previously reported in the literature[1]). Our observations thus seem to corroborate Yoshikawa's model, whereby purely ductile mode removal can be achieved when the mechanism operates at the atomic scale, ductile & fracture mode starts occurring at the interstitial atom vacancy scale, and fully brittle fracture mode transition is observed when the machining unit has progressively increased towards the dislocation/micro-crack scale.

Table 3 Classification of theoretical grinding mechanism and actually observed grinding mode for various pellet types.

Pellet type	Theoretical mechanism	Grinding mode[1]
3μm (resin bond)	Atomic scale	Ductile
9μm (resin bond)	Interstitial atom vacancy	Ductile & fracture
9μm (nickel bond)	Interstitial atom vacancy	Ductile & fracture
40μm (nickel bond)	Dislocation/micro-crack	Fracture

2.6 Evolution of Abrasives over Time

The evolution of the number and shape of the grinding abrasives was investigated by comparing micrographs of the pellets at various time intervals. Figure 11 shows a series of 100x magnification snapshots for the same area of a pellet after respectively 30 min, 2.5 hrs, 5 hrs, and 10 hrs of grinding.

It can be clearly seen that the number and shape of diamonds remains stable throughout the 10 hours of consecutive grinding in this experiment. From this observation, it can be concluded that the removal regime should be stable over long periods of time. This statement supports the stability in volumetric removal rate previously reported in the literature[1].

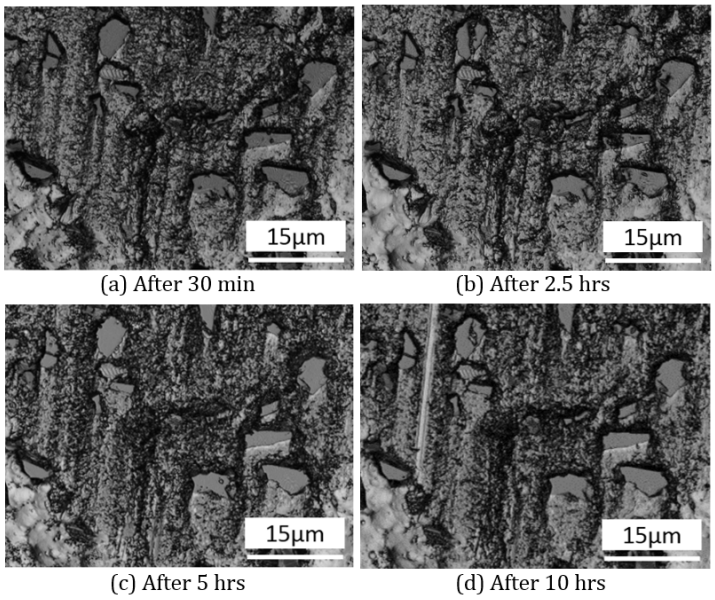

(a) After 30 min (b) After 2.5 hrs

(c) After 5 hrs (d) After 10 hrs

Fig.11 Micrographs of pellet after cumulative grinding time (100x)

3. Study of Grinding Force

3.1 Experimental Method

Another series of experiments were conducted in which the grinding forces were recorded using a dynamometer mounted inside the CNC machine, as shown in Figure 12. The dynamometer was capable of recording grinding forces in both the tangential and normal directions.

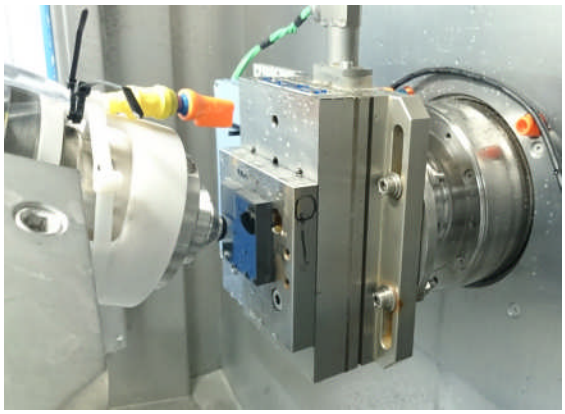

Fig.12 Dynamometer and SAG tool mounted inside the CNC machine

The variable process parameters available on the CNC machine were as follows: the air pressure applied inside the SAG tool, the offsetting of the tool against the workpiece surface (which affects the extent of the grinding area), and the work spindle rotation speed. The range of values used for each parameter is summarized in Table 4.

Table 4 Process parameters of the dynamometric study.

Substrate	Graphite coated with CVD SiC
Tool type	Shape adaptive grinding
Tool radius	10 mm
Tool path mode	Raster
Attack angle	15 deg
Air pressure	0.5 - 2.0 bar
Tool offset	0.05 - 0.35 mm
Spindle rotation	15 - 1500 rpm
Grinding feed	150 mm/min
Abrasives	Diamond
Grain size	3, 9, 40 μm
Pellet material	Nickel and resin

3.2 Results and Analysis

The normal and tangential forces measured with the dynamometer during grinding were subsequently divided by the area of the grinding zone, in order to derive forces per unit of area (N/mm^2). Figure 13 shows, for various grit sizes and pellet materials, the relationship between grinding force and variable process parameters: (a) air pressure inside the SAG tool, (b) tool-offset against the workpiece, and (c) work spindle speed.

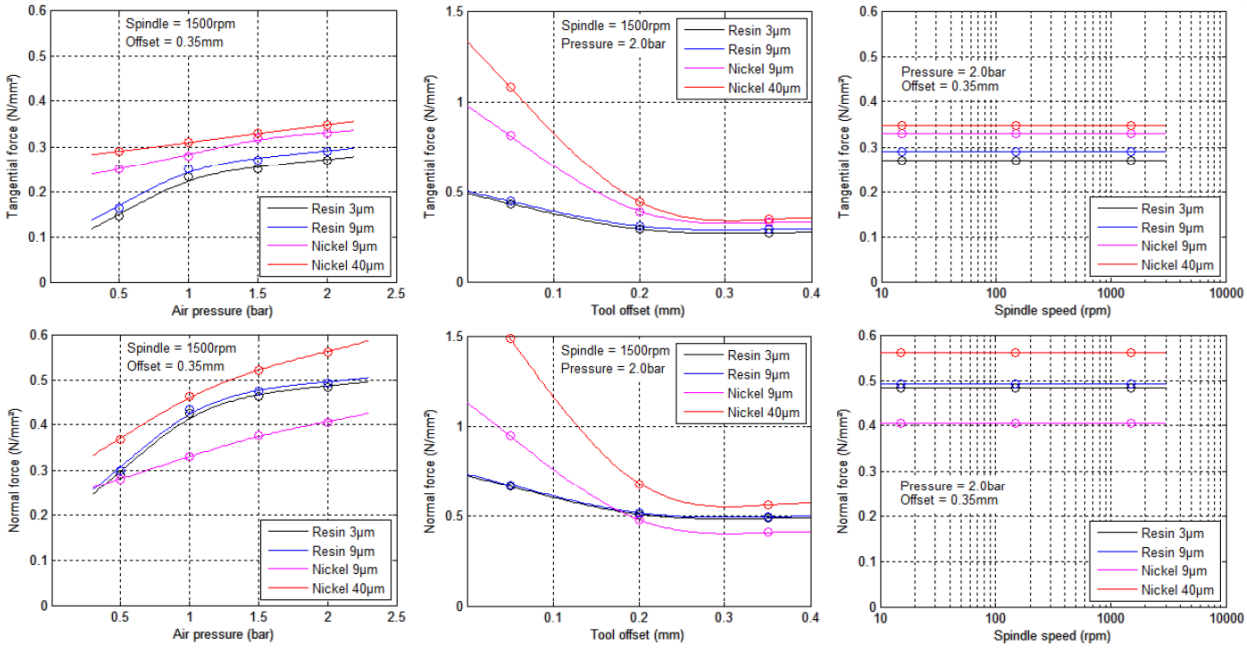

(a) Grinding force vs. air pressure (b) Grinding force vs. tool offset (c) Grinding force vs. spindle speed

Fig.13 Tangential (top) and normal (bottom) grinding forces as function of process parameters

Several observations can be made from these results:

1. In all cases, Fig. 13(a), 13(b) and 13(c), the normal grinding force is slightly higher than the tangential force (by a factor of between x1 and x2).
2. As the diamond grit size becomes higher, both tangential and normal grinding forces also tend to increase accordingly. This result is in contrast with conventional ultra-precision grinding methods, for which the inverse relationship is true[8]. The likely reason for this unusual phenomenon is that the depth of removal in the SAG process is not constrained by the geometrical position of the tool, but is controlled instead by the equivalent dwell time of the grinding area across any given region of the workpiece.
3. Both tangential and normal forces seem to increase linearly with the air pressure (Fig. 13(a)), while the spindle rotation speed has no effect whatsoever (Fig. 13(c)). From this result, it thus appears possible to control the grinding force and removal rate independently of each other, by a combination of air pressure and spindle rotation speed moderation.
4. While the total grinding force increases as a function of tool offset, the force per unit of area follows the inverse relationship as seen in Fig. 13(b) (i.e. the force increases more slowly than the grinding area when the tool offset is being increased). This is likely due to the effect of stresses at the boundary of the contact zone: as the area increases, boundary stresses do not reach any longer the center of the grinding area[9].

Another set of experiments was carried out in which the tangential grinding force was recorded, and the surface roughness of the workpiece was measured between grinding runs with a whitelight interferometer at 10x magnification. It was then possible to correlate the grinding forces with the surface roughness condition of the workpiece, as shown in Fig. 14.

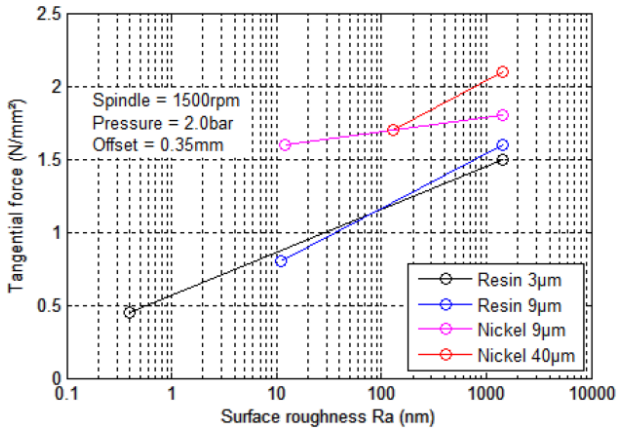

Fig.14 Correlation between tangential force and surface roughness of the workpiece.

It can be seen that a proportional relationship exists between the tangential force and the Ra value of the workpiece roughness. It is expected that the decrease in grinding force reflects a decrease in removal rate, which would occur when the grinding mode transitions from fracture to ductile/fracture and then ductile mode.

3.3 Specific Grinding Energy

The specific energy of the SAG process could also be calculated from the grinding force measurements. The specific energy Kz [J/mm²] is derived from Eq. 4:

$$Kz = \frac{Ft\ Vs}{Q'} \qquad (4)$$

where Ft is the tangential force [N], Vs is the grinding speed [mm/s], and Q' is the volumetric removal rate [mm³/s].

Figure 15 shows the specific energy for the various SAG pellet materials and diamond grit sizes in blue, and compares them with other conventional machining processes in cyan[10, 11]. It can be seen that the average specific energy of the SAG process is one order of magnitude higher than conventional fine grinding. The progressive increase in the specific energy observed as the diamond grit size increases and the pellet binder material becomes softer is in broad agreement with the classification in Table 3, whereby the grinding energy increases as the removal regime transitions from micro-brittle fractures to elasto-plastic deformation in ductile mode.

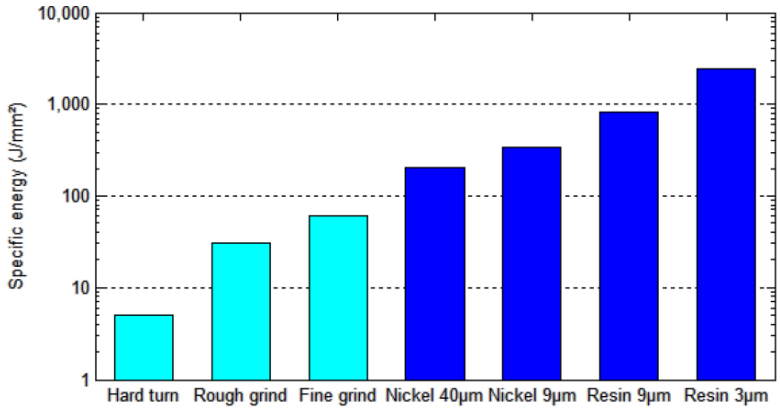

Fig.15 Specific energy of conventional processes (cyan) and SAG process (blue).

4. Conclusions

Plans for future hard X-ray space telescope missions will rely on the ability to produce highly accurate aspheric mandrels for thin mirror replications, with significantly reduced costs when compared to previous missions. An investigation into the mechanism of the novel Shape Adaptive Grinding (SAG) process was presented. By observing pellets under a microscope at various stages of the tool life, it was possible to determine several aspects of the process:

- The number and shape of grinding edges remains stable for over 10 hours of grinding, which helps explain the excellent stability of the volumetric removal rate.
- A negative average rake angle was calculated, which helps explain the longevity of the grinding edges.
- The equivalent chip thickness was determined and used to classify the grinding mechanism

of various pellet types. Ductile mode was associated with atomic level removal, while fracture mode was associated with dislocation/micro-cracks.

- A study of the grinding forces revealed some unique characteristics of this process, such as the ability to control grinding forces and removal rate independently of each other by a combination of air pressure and spindle rotation speed control.

- Finally, it was also established that surface micro-roughness between 0.3 and 0.5 nm Ra can be achieved with this process at various levels of magnification, from AFM to 10x objective.

It is expected that this new technology can be applied in the same manner as the polishing technology used to correctively polish fused silica X-Ray molding dies, for future X-ray telescope missions.

References

[1] Beaucamp A., Namba Y., Combrinck H., Charlton P., Freeman R.: Shape adaptive grinding of CVD silicon carbide, Annals of the CIRP, **63**, 1 (2014)pp.317-320.

[2] Namba Y., Kobayashi H., Suzuki H., Yamashita K.: Ultraprecision surface grinding of chemical vapor deposited silicon carbide for X-ray mirrors using resinoid-bonded diamond wheels, Annals of the CIRP, **48**, 1 (1999)pp.277-280.

[3] Lucca D., Seo Y., Komanduri R.: Effect of tool edge geometry on energy dissipation in ultraprecision machining, Annals of the CIRP, **42**, 1 (1993)pp.83-86.

[4] Inasaki I.: Grinding of hard and brittle materials, Annals of the CIRP, **36**, 2 (1987)pp.463-471.

[5] Snoeys R., Peters J., Decneut A.: The significance of chip thickness in grinding, Annals of the CIRP, **23**, 2 (1974)pp.227-237.

[6] Yoshikawa H.: Brittle-ductile behavior of crystal surface in finishing, Journal of Japan Society of Mechanical Engineers, **35**, 10 (1969)pp.662-667. (in Japanese).

[7] Dobrescu T., Pascu N., Opran C., Bucuresteanu A.: Sub-surface damage in grinding silicon ceramics, Annals of DAAAM, **23**, 1 (2012)pp.121-124.

[8] Namba Y., Abe M.: Ultraprecision grinding of optical glasses to produce super-smooth surfaces, Annals of the CIRP, **42**, 1 (1993)pp.417-420.

[9] Li H., Walker D., Yu G., Sayle A., Messelink W., Evans R., Beaucamp A.: Edges in CNC polishing, paper 2: simulation and validation of tool influence functions on edges, Optics Express, **21**, 1 (2013)pp.370-381.

[10] Davies M., Chou Y., Evans C.: On chip morphology, tool wear and cutting mechanics in finish hard turning, Annals of the CIRP, **45**, 1 (1996)pp.77-82.

[11] Rowe W., Pettit J., Boyle A., Moruzzi J.: Avoidance of thermal damage in grinding and prediction of the damage threshold, Annals of the CIRP, **37**, 1 (1988)pp.327-330.